

Inositol 1,4,5-Trisphosphate 3-Kinase A Is a Novel Microtubule-associated Protein

PKA-DEPENDENT PHOSPHOREGULATION OF MICROTUBULE BINDING AFFINITY[¶]

Received for publication, January 19, 2012, and in revised form, February 29, 2012. Published, JBC Papers in Press, March 2, 2012, DOI 10.1074/jbc.M112.344101

Dongmin Lee[‡], Hyun Woo Lee[‡], Soontaek Hong[‡], Byung-Il Choi[‡], Hyun-wook Kim[‡], Seung Baek Han[‡], Il Hwan Kim[§], Jin Young Bae[¶], Yong Chul Bae[¶], Im Joo Rhyu[‡], Woong Sun[‡], and Hyun Kim^{‡1}

From the [‡]Department of Anatomy, College of Medicine, Korea University, Brain Korea 21, Seoul 136-705, Korea, the [§]Department of Cell Biology, Duke University Medical School, Durham, North Carolina 27710, and the [¶]Department of Oral Anatomy and Neurobiology, School of Dentistry, Kyungpook National University, Brain Korea 21, Daegu, Korea

Background: IP₃K-A mediates synaptic plasticity and memory formation. However, its molecular mechanism is not clear.

Results: Tubulin is identified as an IP₃K-A-binding protein, and PKA reduces the microtubule binding affinity of IP₃K-A.

Conclusion: IP₃K-A is a novel microtubule-associated protein. PKA-dependent phosphorylation negatively regulates interactions between IP₃K-A and microtubule.

Significance: Phosphoregulation of IP₃K-A may serve as its novel regulatory mechanism.

Inositol 1,4,5-trisphosphate 3-kinase A (IP₃K-A) is a brain specific and F-actin-binding protein. We recently demonstrated that IP₃K-A modulates a structural reorganization of dendritic spines through F-actin remodeling, which is required for synaptic plasticity and memory formation in brain. However, detailed functions of IP₃K-A and its regulatory mechanisms involved in the neuronal cytoskeletal dynamics still remain unknown. In the present study, we identified tubulin as a candidate of IP₃K-A-binding protein through proteomic screening. By various *in vitro* and *in vivo* approaches, we demonstrated that IP₃K-A was a novel microtubule-associated protein (MAP), and the N terminus of IP₃K-A was a critical region for direct binding to tubulin in dendritic shaft of hippocampal neurons. Moreover, PKA phosphorylated Ser-119 within IP₃K-A, leading to a significant reduction of microtubule binding affinity. These results suggest that PKA-dependent phosphorylation and microtubule binding of IP₃K-A are involved in its regulatory mechanism for activity-dependent neuronal events such as local calcium signaling and its synaptic targeting.

Inositol 1,4,5-trisphosphate 3-kinase A (IP₃K-A)² was first purified and identified from rat brain, and found to be expressed exclusively in neuronal cells (1, 2). It is distributed in soma, dendrite, and its small protrusion, dendritic spine (3–5). IP₃K-A converts inositol 1,4,5-trisphosphate (IP₃) to inositol 1,3,4,5-tetrakisphosphate (IP₄) to block release of intracellular calcium from endoplasmic reticulum (ER) where IP₃-sensitive calcium channels are located (2, 6). The kinase activity of IP₃K-A is up- or down-regulated by various protein kinases (7,

8). The *in vitro* kinase assay showed that Ser-119 phosphorylation of IP₃K-A by PKA enhances its kinase activity (9, 10), and Ser-185 phosphorylation by PKC reduces its kinase activity (10). In addition, Thr-311 of IP₃K-A is phosphorylated by calmodulin-dependent protein kinase II (CaMKII), enhancing its kinase activity (11), suggesting that diverse signaling pathways are able to regulate enzymatic activity of IP₃K-A. Because of its property as a calcium signaling modulator, classical studies of IP₃K-A have mainly focused on its kinase function. However, recent studies have revealed that IP₃K-A has a novel role for cytoskeletal regulation independent of its kinase function (12, 13). In our recent study, electrophysiology and behavioral tests of IP₃K-A knock-out (KO) mice revealed that IP₃K-A plays an important role in synaptic plasticity and memory formation in brain (13). These findings have encouraged us to consider novel cytoskeleton-related mechanisms of IP₃K-A in synaptic plasticity and memory formation.

IP₃K-A can bind and bundle F-actin via its N-terminal F-actin binding domain (amino acids 1–66) (4), and its bundling effect has been thought to be responsible for structural remodeling of dendritic spine (14, 15). Our recent study also demonstrated that IP₃K-A recruits active Rac1, small GTPase protein, a regulator of actin dynamics (16), into dendritic spine following induction of long-term potentiation (LTP), leading to actin cytoskeleton remodeling in the spine (13). In contrast, glutamate treatment results in its exit from dendritic spines to shafts (14). Synaptic targeting of IP₃K-A is likely to be regulated by the F-actin binding domain only because IP₃K-A L34P mutant protein, lacking F-actin binding, was located mainly in the dendritic shaft rather than dendritic spines (9), suggesting F-actin-mediated synaptic localization of IP₃K-A (14). However, the trigger mechanism for synaptic translocation of IP₃K-A is not yet understood. Here, we report that IP₃K-A is a novel MAP, and PKA-dependent phosphorylation of IP₃K-A negatively regulates interactions between IP₃K-A and microtubule, leading to a dissociation of IP₃K-A from microtubules. These findings may provide the essential mechanism that serves as a spatiotemporal regulation for IP₃K-A.

* This work was supported by the Korea Science and Engineering Foundation (KOSEF) Grant 2011-0019229 (to H. W. L.), 2011-0019227 (to H. K.), and 2010K000830 (to H. K.).

¶ This article contains supplemental Table S1.

¹ To whom correspondence should be addressed: Department of Anatomy, College of Medicine, Korea University, Brain Korea 21, Seoul 136-705, Korea. Tel.: 82-920-6153; Fax: 82-929-5696; E-mail: kimhyun@korea.ac.kr.

² The abbreviations used are: IP₃K-A, inositol 1,4,5-trisphosphate 3-kinase A; MAP, microtubule-associated protein; LTP, long-term potentiation.

EXPERIMENTAL PROCEDURES

Preparations of Constructs and Protein Purification—GST-IP₃K-A-WT was subcloned from previously cloned pEGFP-IP₃K-A-WT (13). The insert of IP₃K-A-WT was amplified by general PCR methods, using primers containing BamHI and EcoRI restriction sites. Deletion mutant and point mutation were carried out by site-directed mutagenesis as previously described (17). Primers used are described in supplemental Table S1. Newly cloned constructs were confirmed by DNA sequence analysis (Macrogen, Republic of Korea). For fusion-protein expression, GST constructs were transformed into *Escherichia coli* BL21 strain (CodonPlus, Stratagene). When optical density (O.D.) reached 0.6–0.8, 0.5 mM IPTG (final concentration) was added to culture media, and they were additionally incubated for 3 h at 25–30 °C. Grown *E. coli* were then collected by centrifugation and suspended in NETT buffer (50 mM Tris-HCl pH 7.4, 100 mM NaCl, 5 mM EDTA, 0.5% Triton X-100, 1 mM DTT) including protease inhibitor mixture (Roche), and sonicated. Then, centrifuged lysates were mixed with washed glutathione-Sepharose beads. After incubation and intensive washes, GST-IP₃K-A proteins were eluted with GST elution buffer (50 mM Tris-HCl pH 8.0, 20 mM reduced glutathione, 0.1% Triton X-100, 1 mM DTT). Finally, GST and GST-IP₃K-A proteins were concentrated with centrifugal filter unit (Millipore).

GST Pull-down Assay—IPTG induced *E. coli* lysates were mixed with glutathione-Sepharose beads. The mixture was incubated overnight in rotator at 4 °C. After washing three times, the Sepharose beads were mixed with rat whole brain lysates. The mixtures were once again incubated for 4 h in a rotator at 4 °C. After intensive washing three times, 2× SDS sample buffer was added, and it was boiled in a heat block for 5 min to separate bound proteins.

MALDI-TOF Analysis—Proper bands in silver-stained gels were selected and carefully excised with no contamination. For MALDI-TOF analysis, selected bands were analyzed commercially by Genomine (Republic of Korea).

Immunoblotting Analysis—After gel electrophoresis, proteins were transferred onto a nitrocellulose membrane (Whatman), and blocked with 5% skim milk in TBST (50 mM Tris-HCl pH 7.4, 150 mM NaCl, 0.1% Tween20) for 30 min. Then, the membrane was incubated with primary antibodies for 1 h at room temperature or overnight at 4 °C. After washing three times, the membrane was incubated with horseradish peroxidase (HRP)-conjugated secondary antibody for 30 min and developed using the ECL system (Thermo Scientific Pierce).

Microtubule Co-sedimentation Assay—We used microtubule-binding protein co-sedimentation assay kit (Cytoskeleton, BK029) as the manufacturer's manual described. In brief, we suspended the purified protein in general tubulin buffer (80 mM PIPES pH 7.0, 2 mM MgCl₂, 0.5 mM EGTA), 1 mM GTP and 20 mM taxol were added, and the reactions incubated at room temperature for 30 min. 100 μl of the cushion buffer were placed into each tube, and each reaction mixture was carefully layered on top of the cushion buffer. We centrifuged each tube at 100,000 × *g* at room temperature for 40 min. For further anal-

ysis, some supernatant was kept. We resuspended the pellet in SDS sample buffer for immunoblotting analysis.

Immunoprecipitation—We sacrificed 12-week-old male rats by cervical translocation, then quickly removed the skull and dissected the whole brain without any damage. We prepared whole brain lysate in NETN buffer (50 mM Tris-HCl pH 7.4, 100 mM NaCl, 5 mM EDTA, 0.5% Nonidet P-40, 1 mM DTT, protease inhibitor mixture), by 10 strokes of Teflon-glass homogenization and sonication. After centrifugation at 10,000 × *g* for 20 min to remove cell debris, the supernatant was transferred to protein G beads for the pre-clearing procedure. Mixtures of lysate and protein G beads were incubated at 4 °C for 30 min to reduce nonspecific binding. After centrifugation at 10,000 × *g* for 20 min, the supernatant was transferred to fresh tubes, and 10 μg of either normal mouse IgG or anti-IP₃K-A (VI5G) was then added to the pre-cleared lysates. The mixtures of lysate and antibody were incubated for 4 h at 4 °C. Then, this mixture and washed protein G beads were additionally incubated in a rotator at 4 °C for 4 h. After intensive washing three times, 2× SDS sample buffer was added, and the mixtures were boiled in a heat block for 5 min to separate bound proteins.

Tissue-based Microtubule Co-sedimentation Assay—We carried out tissue-based microtubule co-sedimentation assay as previously described (18), with some modification. Briefly, we rapidly dissected rat or mouse whole brain and prepared lysates using Teflon-glass homogenizer in general tubulin buffer. After sonication and centrifugation at 10,000 × *g* for 10 min at 4 °C, the lysates were incubated for 1 h on ice. We performed the first ultracentrifugation at 100,000 × *g* at 4 °C for 1 h, and kept cleared supernatant for the next step. The supernatant was mixed with 1 mM GTP and 20 μM taxol for microtubule polymerization, and the mixture was then incubated for 30 min at 37 °C. Finally, we performed the second ultracentrifugation at 100,000 × *g* for 1 h at 25 °C. For immunoblotting analysis, supernatant was transferred into fresh tubes, then pellets were resuspended with SDS sample buffer. For immunofluorescence analysis, pellets were collected into poly-D-lysine (PDL)-coated plastic coverslips (SPL, 20009) during ultracentrifugation. Plastic coverslips were placed on homemade silicon spacers to prevent their deformation. The general experimental protocol steps are described schematically in Fig. 3A.

Immunocytochemistry—Hippocampal culture neurons were fixed with pre-warmed 4% paraformaldehyde in phosphate-buffered saline (PBS; Biosesang, pH 7.4). Neurons were permeabilized with 0.1% Triton X-100 in TBS, incubated with 5% bovine serum albumin in TBST for 1 h, and then incubated with primary antibodies in TBST for 1 h at room temperature or overnight at 4 °C, followed by incubation with fluorophore-conjugated secondary antibodies in TBST for 30 min. After washing three times, coverslips were mounted with a mounting solution (Biomedica).

Immunogold Labeling—Sprague-Dawley adult male rat (8 weeks of age) was anesthetized deeply with sodium pentobarbital (100 mg/kg) and transcardially perfused with a fixative contacting 2% paraformaldehyde and 2.5% glutaraldehyde in 0.1 M phosphate buffer (PB; pH 7.4). The hippocampus region was dissected from the brain and stored in the same fixative for 24 h at 4 °C. The samples were post-fixed in 1% osmium tetrox-

ide, dehydrated through an ascending ethanol series, and embedded with an Epon mixture. Thin sections (90 nm) were obtained using a Reichert-Jung Ultracut E ultramicrotome (Leica, Germany), and mounted on 200 mesh nickel grids. Postembedding immunogold labeling was performed according to the procedure described (19, 20) with some modifications. Briefly, the grids were dipped for 10 min in 1% periodic acid and for 15 min in 9% sodium periodate. They were washed with distilled water gently several times and transferred to Tris-buffered saline containing 0.1% Triton X-100 (TBST, pH 7.4) for 10 min. The samples were incubated with 2% human serum albumin (HAS) for 10 min, and transferred to anti-IP₃K-A (II4E, 1:200) in TBST containing 2% HAS for 3 h at room temperature. After extensive rinsing in TBST, the grids were incubated for 1 h with goat anti-mouse IgG-conjugated 15 nm gold particles (1:25 in TBST containing 0.05% polyethylene glycol; EMS). After washing with distilled water, the grids were stained with uranyl acetate and lead citrate, and observed under Hitachi H-7500 electron microscope (Hitachi, Japan).

Cryofixation, Cryosubstitution, and Low Temperature Embedding—Coronal vibratome sections (300 μm) were cryoprotected by immersing them in increasing concentrations of glycerol (10, 20, and 30% in 0.01 M PBS, pH 7.4) for 30 min at each concentration at room temperature in 30% glycerol overnight at 4 °C. Sections were placed on the specimen pin and plunged into liquid propane at −170 °C by cooled liquid nitrogen (Leica EM CPC, Bannockburn, IL). For cryosubstitution and low-temperature embedding, sections were transferred to Leica EM AFS and treated as follows: 24 h in 0.5% uranyl acetate in absolute methanol (−90 °C) and stepwise-raised temperature with 4 °C increments per hour from −90 °C to −45 °C; wash the sections three times with absolute methanol (this and the following at −45 °C); 2 h each in 50, 75, and 100% Lowicryl HM20, and two times for 12 h each in 100% Lowicryl. Sections were then polymerized with UV light (48 h at −45 °C, 48 h at 0 °C, and 48 h at +20 °C). The CA1 area of the hippocampus was excised and glued to EM blocks. Ultrathin sections were obtained (90 nm) and collected on 200 mesh nickel grids.

Transfection into HEK293 Cells—GFP-IP₃K-A constructs were transfected into HEK293 cells with Lipofectamine 2000 (Invitrogen) according to the manufacturer's instructions.

Production of IP₃K-A Ser-119 Phosphoantibody—Phosphopeptide of sequence QPRRL(pS)TSSLSS was used as an antigen for IP₃K-A Ser119 phosphoantibody. This antibody was produced commercially by AbFrotier (Republic of Korea).

Kinase Reaction with PKA Catalytic Subunit—Eluted GST-IP₃K-A proteins were phosphorylated with PKA catalytic subunit (New England Biolabs; P6000S) for 2 h at 30 °C. The reaction conditions were: 50 mM Tris-HCl, pH 7.5, 10 mM MgCl₂, 200 μM ATP, and 20,000 units of PKA catalytic subunit.

Antibodies and Reagents—The following primary and secondary antibodies were used in immunoblotting analysis: mouse anti-IP₃K-A antibody (homemade II4E; 1:2000), rat anti-IP₃K-A Ser-119 phosphoantibody (homemade; 1:1000), mouse anti-tubulin βIII (Sigma-Aldrich; T8660; 1:2500), mouse anti-tubulin α (Santa Cruz Biotechnology; SC-8035; 1:2500), mouse anti-β-actin (Sigma-Aldrich, A5441; 1:5000), mouse anti-GFP (Santa Cruz Biotechnology; SC-9996; 1:2500),

mouse anti-GAPDH (Santa Cruz Biotechnology; SC-32233; 1:2500), rabbit anti-pS845 GluRI (Millipore; 04-1073; 1:1000), mouse anti-GST (homemade; 1:2500), mouse anti-IgG HRP (Jackson Lab; 1:10,000), mouse anti-IgG light chain specific HRP (Jackson Lab; 1:10,000), mouse anti-IgM HRP (Jackson Lab; 1:10,000), rat anti-IgG HRP (Jackson Lab, 1:10,000), and rabbit anti-IgG HRP (Jackson Lab, 1:10,000). The following reagents were used in this study: taxol (Cytoskeleton; TXD01), GTP (Cytoskeleton; BST06), protease inhibitor (Roche; cOmplete Mini EDTA-free), protein phosphatase inhibitor mixture tablet (Roche; PhosSTOP), lambda protein phosphatase (New England Biolabs; P0753S), forskolin (Sigma-Aldrich; F6886), H-89 (Sigma-Aldrich; B1427), and purified bovine tubulin (Cytoskeleton; TL238).

Cell Culture—HEK293 cells were grown in Dulbecco's modified Eagle's medium (DMEM), containing 10% fetal bovine serum and 1% penicillin-streptomycin (Invitrogen), according to general mammalian cell culture methods. The cell incubator was set and maintained at 37 °C and 40~70% humidity. Primary hippocampal neuron culture was performed as previously described (13). Briefly, rat hippocampus (embryonic, 18~19 day) was rapidly dissected and digested with 0.25% trypsin-EDTA (Invitrogen). Digested cells were plated on 50 μg/ml PDL (Sigma-Aldrich) pre-coated coverslips. Media consisted of neurobasal medium (Invitrogen) and following reagents; 0.5 mM L-glutamine (Invitrogen), 25 mM glutamic acid (Sigma-Aldrich), 1:50(v/v) B27 supplement (Invitrogen), and antibiotics.

Immunoblotting Densitometric Analysis and Image Processing—Immunoblotting images were measured by ImageJ (NIH) software, and all images and data were processed by Photoshop CS5 (Adobe) and Illustrator CS5 (Adobe) software.

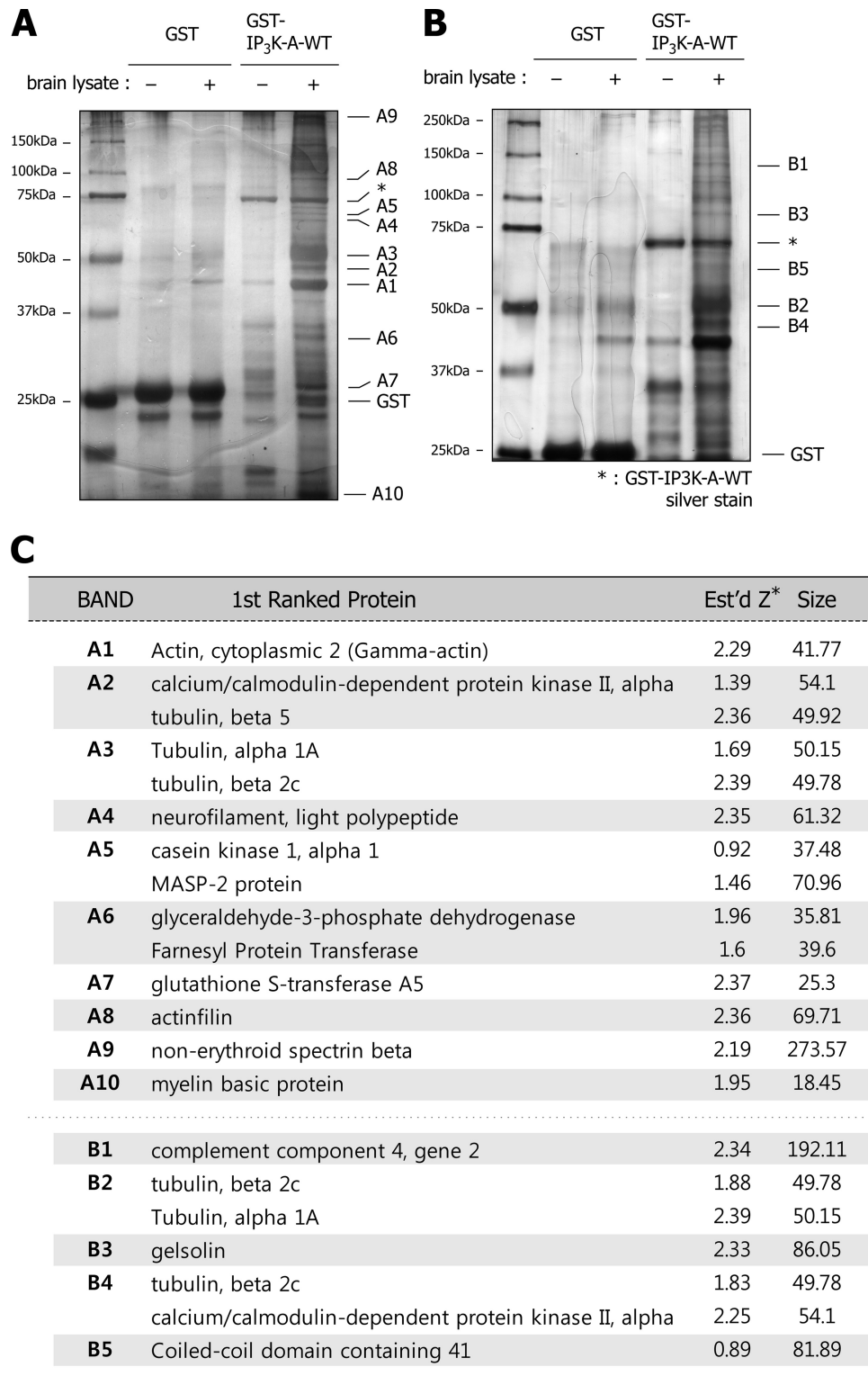
Statistical Analysis—For quantitative analysis, we used Student's *t* test and one-way ANOVA by SPSS 12.0K (IBM SPSS) software. Dunnett's test was used for *post hoc* test.

RESULTS

Tubulin Is Identified as a Novel Binding Partner of IP₃K-A—To further understand the role of IP₃K-A in neurons, we tried to find novel binding partners that could be related to hitherto-unknown functions or mechanisms of IP₃K-A. For this, we used glutathione *S*-transferase (GST)-fused IP₃K-A proteins. Silver-stained SDS-PAGE gels from the pull-down assay displayed several clear bands that were detected only in the GST-IP₃K-A-WT lane, which were supposed to be the binding candidates (Fig. 1, A and B). The selected bands were excised, and analyzed by MALDI-TOF (matrix-assisted laser desorption ionization-time of flight mass spectrometry) method. Identified results included previously reported IP₃K-A binding proteins such as actin (A1) and CaMKIIα (A2 and B4) (Fig. 1C) (4, 11), suggesting that our screening system worked properly. In the list of MALDI-TOF analysis, tubulin (A2, A3, B2, and B4), the subunit of microtubule, was the most noticeable candidate. Because some F-actin-binding proteins also associate with microtubules or *vice versa* (21–27) and recent studies suggest that IP₃K-A strongly related neuronal cytoskeleton, we selected tubulin as the first candidate for our study.

IP₃K-A Binds Directly to Microtubules—To test specific interaction between IP₃K-A and tubulin, we performed GST

IP₃K-A Binds Microtubule by PKA Phosphoregulation



* Z score of 1.282 = 90.0%, 1.645 = 95.0%, and 3.090 = 99.0%

FIGURE 1. **MALDI-TOF analysis of GST-IP₃K-A pull-down assay.** A and B, silver-stained gel images of GST pull-down samples. We used both 10% (A) and 8% (B) acrylamide gels to cover a wide range of candidates. Bands of interest, which are shown only in the GST-IP₃K-A-WT lane, were denoted as A1~A10 and B1~B5. Denoted bands were excised from gels for MALDI-TOF analysis. Asterisks indicate each purified GST-IP₃K-A-WT. C, table represents the results of MALDI-TOF analysis. The Z score is a probability value that a candidate in a database is the protein being analyzed. The higher Z score means more correct identification (Z score of 1.282 = 90.0%, 1.645 = 95.0%, and 3.090 = 99.0%).

pull-down assays with increasing levels of GST-IP₃K-A protein, and found that the intensity of tubulin bands correlated well with loading levels of GST-IP₃K-A (Fig. 2A), suggesting that

IP₃K-A specifically associates with tubulin. Because the pull-down assay does not necessarily confirm a direct interaction between IP₃K-A and tubulin, we performed *in vitro* microtu-

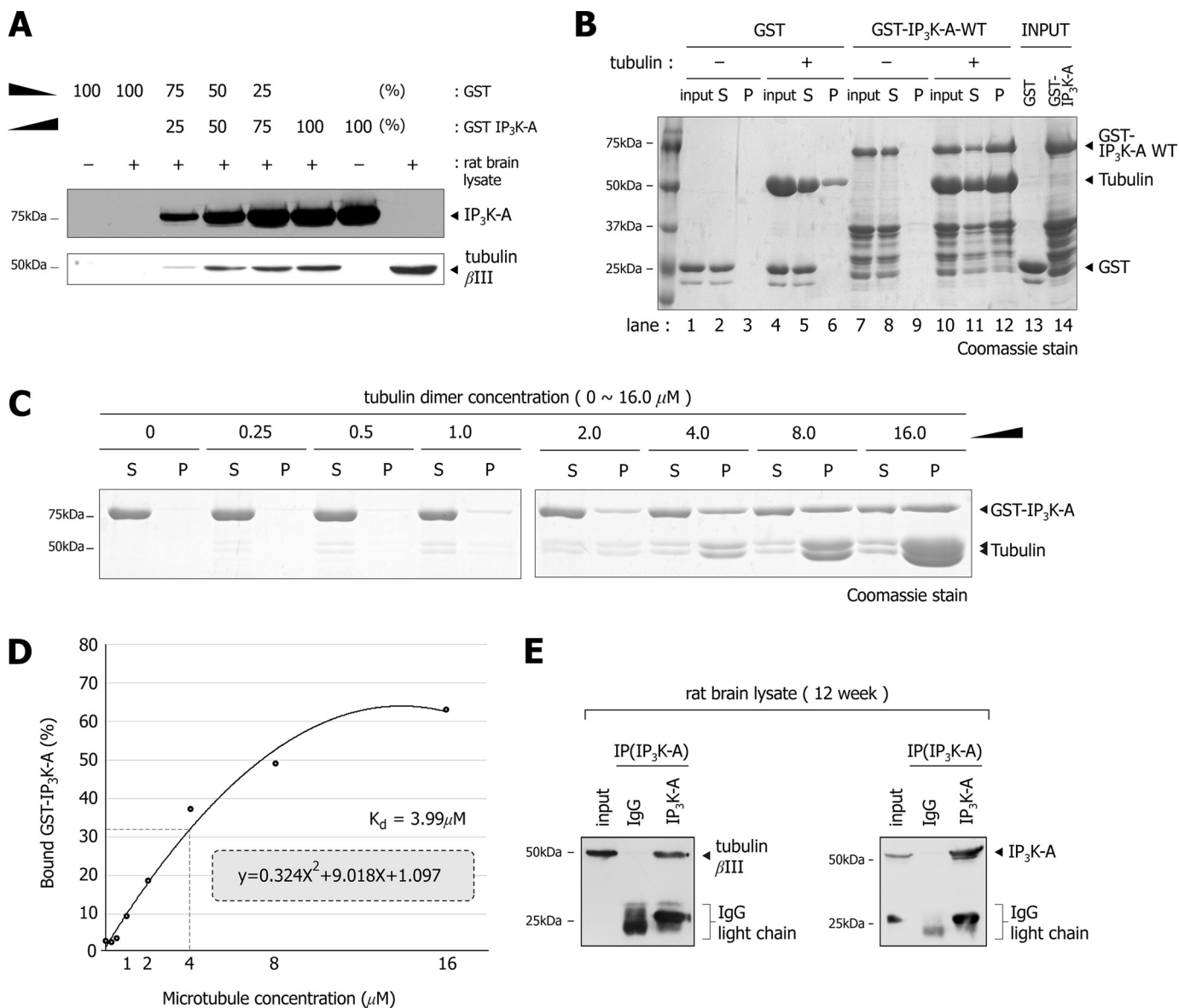


FIGURE 2. **GST-IP₃K-A binds directly to microtubules.** *A*, immunoblot analysis of the GST pull-down assay with increasing GST-IP₃K-A protein levels. Note that the intensity of tubulin βIII blots is increasing as GST-IP₃K-A is increased, and GST is decreased. *B*, Coomassie-stained gel image of *in vitro* microtubule co-sedimentation assay. Purified GST-IP₃K-A and GST were mixed with purified tubulin in addition to GTP and taxol, which are necessary in microtubule polymerizations and stabilization. GST-IP₃K-A cosedimented with tubulin dimer, but GST control was not pelleted, regardless of tubulin. *C*, Coomassie-stained gel image of the *in vitro* microtubule co-sedimentation assay with increasing concentrations of microtubules. A constant concentration of 1.0 μM GST-IP₃K-A was mixed and incubated with increasing concentrations (0 to 16.0 μM) of microtubules. As concentrations of tubulin dimer increased, bands of IP₃K-A shifted from supernatant (S) to pellet (P) fractions. *D*, IP₃K-A binding curve to microtubules. This curve was obtained by plotting densitometric analysis of Fig. 2B. We assumed the dissociation constant (K_d) to be 3.99 μM. *E*, immunoblots of immunoprecipitation assay. Tubulin was precipitated by anti IP₃K-A monoclonal antibody (V15G).

bule co-sedimentation assay. Fig. 2B shows that purified GST-IP₃K-A cosedimented with microtubules, but not GST control, indicating that GST-IP₃K-A binds directly to microtubule. In addition, constant concentrations of GST-IP₃K-A were shifted from supernatant (S) to pellet (P) portions with increasing concentration of microtubule (Fig. 2C), further confirming that IP₃K-A binds directly to microtubules. The microtubule binding curve was drawn by the densitometric analysis of GST-IP₃K-A, and dissociation constant of 3.99 μM was obtained from the binding curve (Fig. 2D). Immunoprecipitation assay revealed that endogenous IP₃K-A also interacts with microtubules in rat brain (Fig. 2E). Conversely, we physically pulled

microtubule down by tissue-based co-sedimentation assay, which is illustrated schematically in Fig. 3A. We investigated the presence of IP₃K-A in MAP-enriched pellets using both immunoblotting and immunofluorescence analysis. In immunoblotting analysis, endogenous IP₃K-A was pelleted better when mixed with taxol, a well-known microtubule stabilizer, than without it (Fig. 3B). These taxol-dependent co-sedimentations of IP₃K-A were also found in immunofluorescence analysis (Fig. 3, C–K). Co-localizations of IP₃K-A and microtubules were increasingly evident in the taxol-treated group (Fig. 3, F–H) than in the control group (Fig. 3, C–E). However, we did not observe any immunoreactivity of IP₃K-A antibody in the

IP₃K-A Binds Microtubule by PKA Phosphoregulation

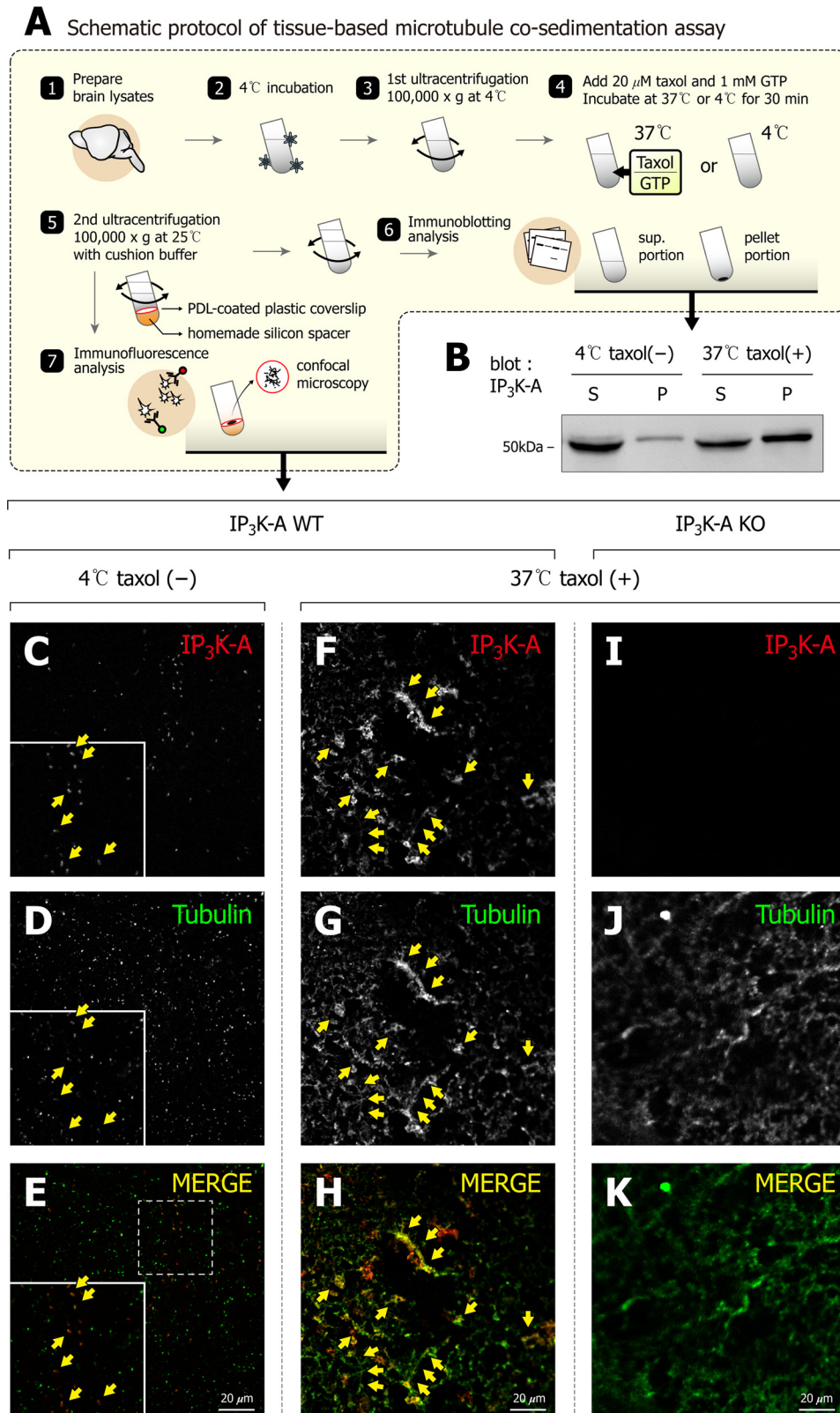


FIGURE 3. Taxol-dependent co-sedimentation of tubulin and IP₃K-A. **A**, schematic figure which describes experimental steps of general protocols about tissue-based microtubule co-sedimentation assay. Specific pelleting of IP₃K-A was confirmed by both immunoblot and immunofluorescence assay. **B**, immunoblot analysis of tissue-based microtubule co-sedimentation assay. Note that endogenous IP₃K-A were more pelleted in the taxol-treated group than in the control group. **C–K**, representative immunofluorescence images of tissue-based microtubule co-sedimentation assay. Microtubules and MAPs were collected on PDL-coated plastic coverslips during ultracentrifugation, then coverslips were double-labeled by anti-IP₃K-A antibody (red) and anti-tubulin antibody (green). Yellow arrows indicate prominent co-localization between IP₃K-A and microtubules. Scale bar: 20 μm.

group of IP₃K-A knock-out mouse (Fig. 3I), indicating that the IP₃K-A antibody was reliable. These findings strongly suggest that endogenous IP₃K-A binds to microtubules.

IP₃K-A Distributes along Microtubule in Vivo Rat Brain Sections and Primary Culture Neuron—We next examined the fine localization of IP₃K-A by both immunocytochemistry and immunogold electron microscopy. In cultured hippocampal neurons, IP₃K-A immunofluorescence signals were detected mainly in soma, dendrite, and dendritic spine (Fig. 4, A and B), consistent with previous reports (3–5). IP₃K-A distributed mainly along dendritic shafts in immature neurons (div 10; Fig. 4A), while synaptic localization of IP₃K-A was evident in mature neurons (Fig. 4D). Next, we examined the ultra-structural localization of IP₃K-A protein in rat brain region by immunogold electron microscopy using rat brain slices (8-week-old). In electron microscopic images, microtubule structures are readily distinguished by prominent structures with typical width, 24 nm. In this study, IP₃K-A signals distributed on cross-section of microtubules (Fig. 4G), but not in vascular structures and void spaces (data not shown), indicating that IP₃K-A antibody provides a reliable specificity. These results show that IP₃K-A is present in dendritic microtubule in hippocampus *in vivo*.

IP₃K-A Binds to Microtubule via Its N-terminal Region—To identify essential microtubule binding regions in IP₃K-A, we first checked using partial GST-IP₃K-A constructs containing N terminus (aa 1–190) and C terminus (aa 191–459) sequences.³ In this pull-down assay, we observed that tubulin was pulled by only the N terminus construct, but not by C terminus (data not shown), indicating that microtubule binding regions of IP₃K-A are located at the N terminus. To further determine the specific regions essential for microtubule binding, we generated various GST-IP₃K-A constructs (Fig. 5A). In pull-down assays, deletion mutants of Δ12–42, Δ64–105, and Δ67–161 did not form complexes with microtubules, and Δ132–160 and Δ161–193 showed reduced interactions compared with wild type (Fig. 5C), suggesting that IP₃K-A has multiple microtubule binding regions along amino acids 12–42, 64–105, 132–160, and 161–193 (Fig. 5D). Even though the tubulin binding region of IP₃K-A turned out to be complex and it was hard to define the exact regions, the overall GST pull-down data provided valuable information on the domains that are involved in the interaction between IP₃K-A and tubulin.

Microtubule Binding of IP₃K-A Is Regulated by Phosphorylation of IP₃K-A Ser119—In our preliminary microtubule co-sedimentation assay, IP₃K-A expressed in mammalian cells were less pelleted than bacterially expressed IP₃K-A (data not shown), implying that this discrepancy might be due to post-translational modifications such as phosphorylation. Notably, there is numerous experimental evidence to indicate that phosphorylation of MAPs regulates their microtubule binding affinity; for example, tau, microtubule-associated protein 2 (MAP2), and doublecortin (28–31). Previous studies reported that

IP₃K-A can be phosphorylated at Ser-119 by PKA (9), Ser-119 and Ser-185 by PKC (9), and Thr-311 by CaMKII (11). Among them, Ser-119 is flanked by defined microtubule binding regions (Fig. 6A), and this sequence contains the consensus sequence (RRXS) of PKA substrates and is well conserved among mouse, rat, and human (Fig. 6A). Therefore, we examined whether IP₃K-A binding affinity toward microtubule is regulated by Ser-119 phosphorylation. For this, we overexpressed GFP-IP₃K-A wild type (WT) and a phosphodeficient form (S119A) in HEK293 cells, and then performed tissue-based microtubule co-sedimentation assay to measure their binding affinity. Additionally, we tested the effect of forskolin, which increases the intracellular cAMP and induces PKA activation (32). We found that GFP-IP₃K-A-WT (lanes 2 and 4) was less pelleted than GFP-IP₃K-A-S119A (lanes 6 and 8), and forskolin significantly reduced the pellet portion of wild type (lanes 2 and 4), but not of S119A (lanes 6 and 8) in parallel experiments (Fig. 6, B and D). However, the amounts of pelleted tubulin in all experimental samples were not affected (Fig. 6, C–E). These results suggest that Ser-119 might play a role in microtubule binding via phosphorylation by PKA.

PKA Regulates the Microtubule Binding Affinity of IP₃K-A—Earlier studies together with our present results suggest that PKA directly phosphorylates IP₃K-A at Ser-119 (9). How is the microtubule binding of IP₃K-A regulated by PKA-mediated intracellular phosphorylation at Ser-119? To obtain cellular evidence, we tried to determine the Ser-119 phosphorylation level by PKA activity. For this, we first generated polyclonal antibody (αpSer119) against phosphopeptide that encompasses the putative phosphorylation residue at Ser-119. This antibody revealed two major bands in the brain (~70 and ~50 kDa), and the lower band was not detected in the brain lysate of IP₃K-A KO mice (Fig. 7A), suggesting that our phosphoantibody could specifically detect endogenous IP₃K-A. In hippocampal-cultured neurons, forskolin treatment enhanced the band intensity compared with control, which was not detectable by the treatment of lambda protein phosphatase (λPP) (Fig. 7B). In addition, exogenous GFP-IP₃K-A-WT expressed in HEK293 cells was detected by αpSer119 but not GFP-IP₃K-A-S119A mutant (Fig. 7, C and D), demonstrating that αpSer119 detects phosphorylation of IP₃K-A at Ser-119, which is closely related to the PKA pathway.

To obtain further cellular evidence, we examined Ser-119 phosphorylation levels in HEK293 cells co-transfected with GFP-IP₃K-A and PKA catalytic β-subunit wild type or an inactive mutant (33) (Fig. 8A, *upper blot*). When HEK293 cells transfected singly with GFP-IP₃K-A-WT were immunoblotted with αpS119 antibodies, a significant amount of phosphorylated IP₃K-A was detected, suggesting that significant portions of IP₃K-A were basally phosphorylated in HEK293 cells. IP₃K-A phosphorylation was slightly increased upon co-expression with PKA catalytic subunit wild type, whereas phosphorylation was reduced by co-expression with an inactive catalytic subunit. In hippocampal culture neuron, H-89, a potent PKA inhibitor, blocked Ser-119 phosphorylation even in the forskolin treatment (Fig. 8B). These results together indicate that PKA directly phosphorylates IP₃K-A at Ser-119 *in vivo* as well as *in vitro*. We next investigated how microtubule binding was reg-

³ The amino acid numbering of the present study was done from rat sequences of IP₃K-A. Note that amino acid sequences of human IP₃K-A have two additional amino acids (Pro-89 and Ser-112) compared to the rodent.

IP₃K-A Binds Microtubule by PKA Phosphoregulation

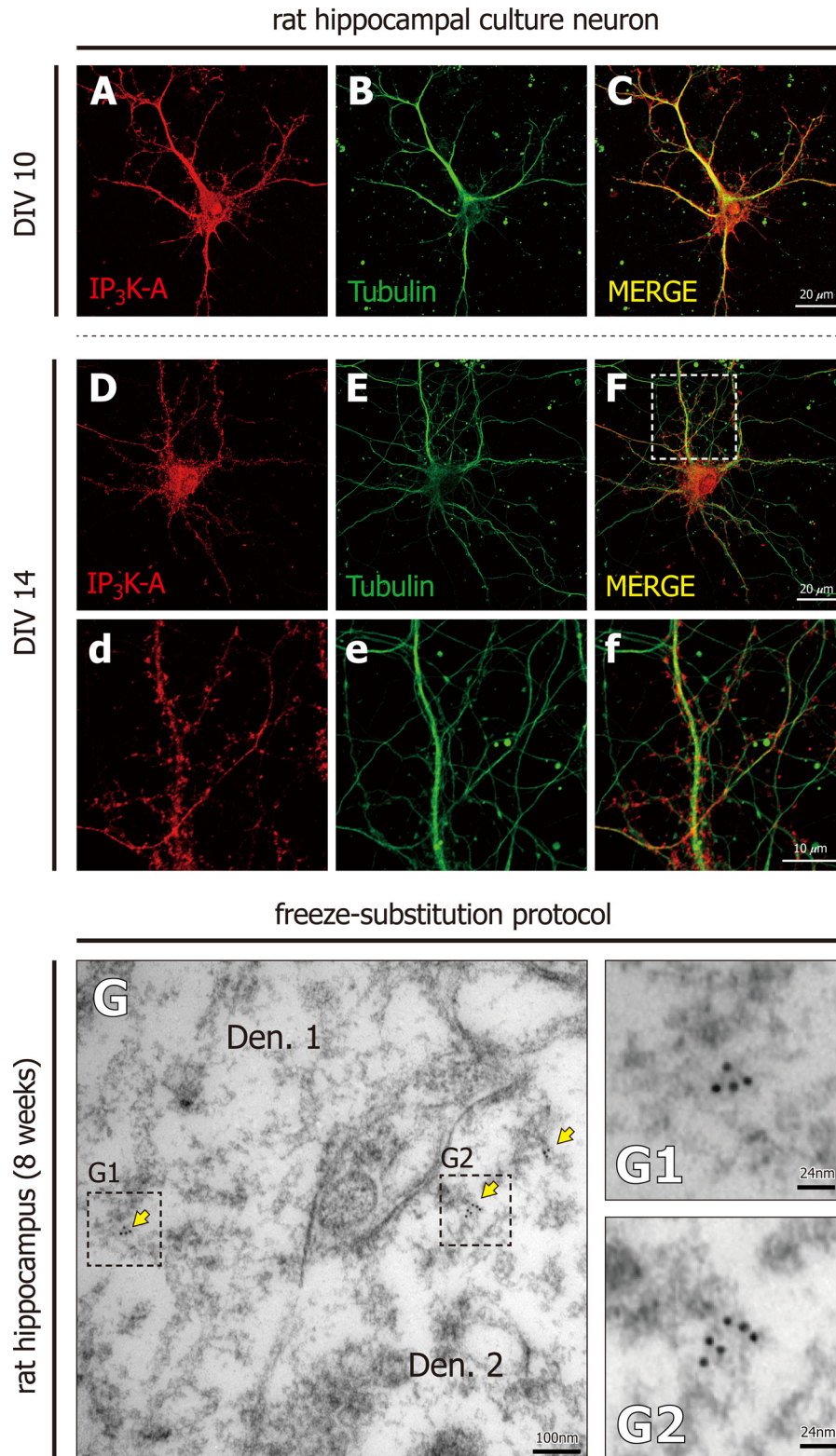


FIGURE 4. IP₃K-A distributes along microtubule structure, shown by immunocytochemistry and immunogold electron microscopy. Representative images of rat hippocampal neurons (A–C: div 10, D–F: div 14) and double-labeled with anti-IP₃K-A antibody (red) and anti-tubulin antibody (green). Scale bar: 20 μ m (d–f). Magnified images of Fig. 3, D–F. Scale bar: 10 μ m. G and H, representative immunogold electron microscopic images. IP₃K-A specific antibody and gold particle-tagged secondary antibody were applied to the sections of 8-week-old rat brain. Sections were prepared by a freeze substitution method. IP₃K-A-labeled gold particles (yellow arrow; G: gold particle diameter 6 nm) distributed on cross-sectional side of microtubules. Den, dendrite; Scale bar: G, 200 nm; (G1, G2) Magnified images of Fig. 3G. Scale bar: G1 and G2, 34 and 100 nm.

ulated by PKA-dependent phosphorylation. We mixed purified PKA catalytic subunit with purified GST-IP₃K-A proteins (wild type and S119A mutant), and performed a co-sedimentation

assay. The PKA catalytic subunit significantly reduced the pellet portion of IP₃K-A wild type (Fig. 8, C and E; lane 4), but not S119A (Fig. 8, C and E; lane 8), phosphodeficient form, consist-

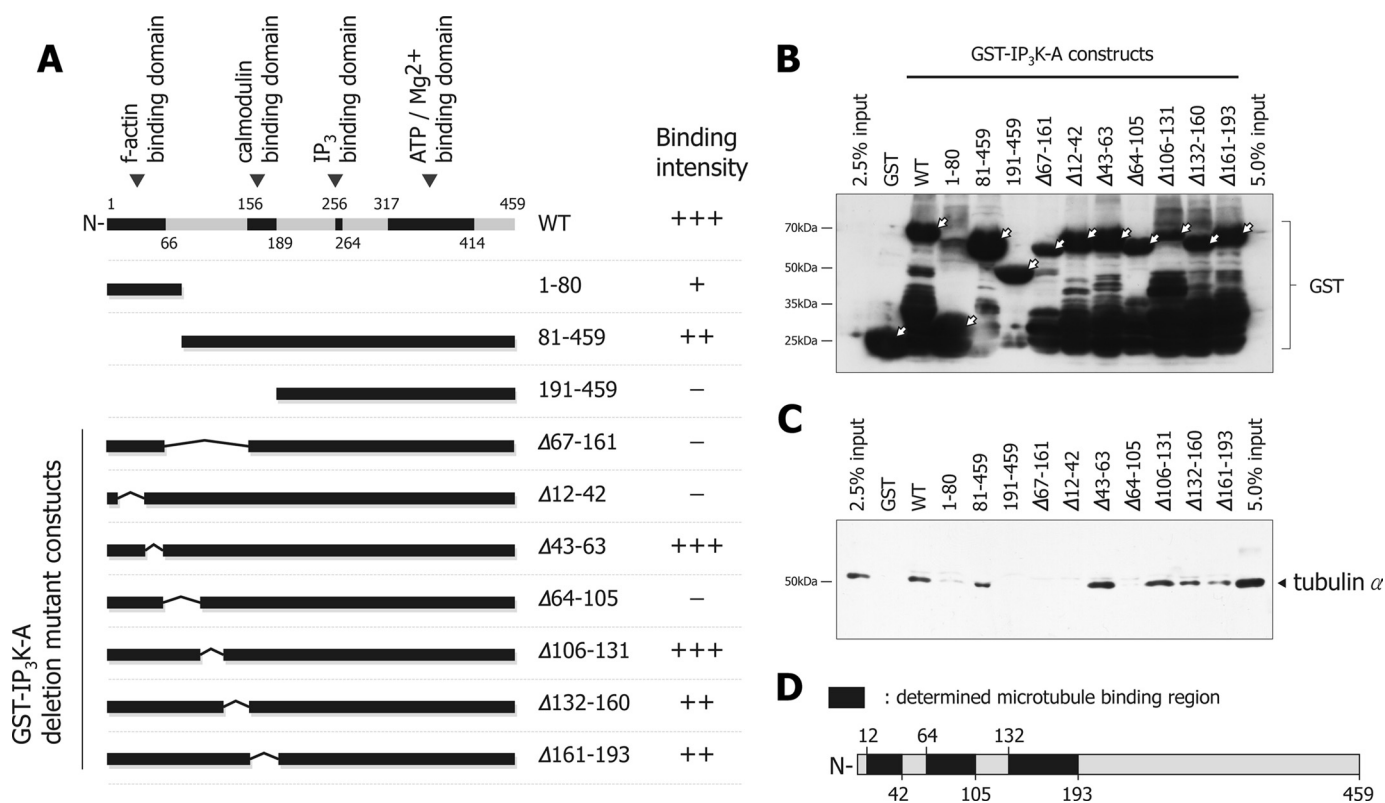


FIGURE 5. Determination of microtubule binding regions within IP₃K-A. *A*, schematic figure depicts various constructs of GST-IP₃K-A which were used in microtubule binding regions mapping assay. Protein-coding regions are depicted by *solid bars* and non-coding regions by *bent lines*. Numbers within the construct name denote the amino acid number from the N terminus. Constructs were designed to determine whether deletion regions or fragmented regions were essential components for microtubule binding. Microtubule binding intensity of each construct is presented by a + or - symbol. *B*, immunoblotting image of GST pull-down assay by GST antibody. By blotting with GST specific antibody, we checked the expression level of GST alone and GST-IP₃K-A constructs (*white arrows* indicate fully expressed constructs). All constructs were detected at the expected size. *C*, immunoblotting image of GST pull-down assay with tubulin α antibody. Tubulin-specific bands were not detected in 191-459, Δ 67-161, Δ 12-42, and Δ 64-105 lanes. Additionally, 1-80, Δ 132-160, and Δ 161-193 are shown to have lower band intensities, compared with WT. To rule out the effect of dimerization by endogenous IP₃K-A, we used IP₃K-A knock-out mouse brain lysate. *D*, schematic figure indicates defined microtubule binding regions; 12-42, 64-105, 132-160, and 161-193.

ent with the results shown in Fig. 5. The PKA activity was verified by the amount of pSer119 IP₃K-A level compared with total IP₃K-A. We found a significant increase of phosphor-IP₃K-A by PKA in GST-IP₃K-A WT, but not in the S119A mutant (Fig. 8D). For quantification, we developed a new equation for the microtubule-enriched fractionation coefficient (MTeF-coefficient) (Fig. 8F). The higher MTeF-coefficient indicates stronger microtubule binding affinity. As seen in Fig. 8F, quantitative analysis showed that GST-IP₃K-A-WT treated with PKA had lower MTeF-coefficient compared with control. In contrast, two groups of GST-IP₃K-A-S119A had similar MTeF-coefficients regardless of PKA treatment, further confirming that PKA-dependent Ser-119 phosphorylation of IP₃K-A directly inhibits its interaction with microtubules.

Phosphorylated Endogenous IP₃K-A Has Lower Binding Affinity toward Microtubules—Forskolin reduced the microtubule binding affinity of GFP-IP₃K-A-WT in microtubule co-sedimentation assay, but not GFP-IP₃K-A-S119A (Fig. 6), and increased the phosphorylation of IP₃K-A Ser-119 (Fig. 8B), suggesting that PKA-dependent phosphorylation of Ser-119 weakens microtubule binding affinity of IP₃K-A. Accordingly, we monitored whether Ser-119 phosphorylation status of endogenous IP₃K-A affected its microtubule binding. We performed tissue-based microtubule co-sedimentation assay for microtubule-enriched fractionation. Because our α pSer119 detected

some nonspecific bands, we used both IP₃K-A-WT and KO mouse brain lysates to distinguish the real IP₃K-A band. Total IP₃K-A was detected in both supernatant (Fig. 9A, lane 2), which is not associated with microtubule, as well as the pellet portion (Fig. 9A, lane 6), which is bound to microtubule. However, IP₃K-A pSer119 was detected only in the supernatant portion (Fig. 9B, lane 2), but not in the pellet portion. The integrity of microtubule-enriched fractionation was verified by immunoblotting with tubulin β III and β -actin, indicating that these fractions included only microtubule and its binding proteins but not F-actin (Fig. 9C). We then determined MTeF-coefficients of both total IP₃K-A-detected bands ($34.25 \pm 4.08\%$; mean \pm S.E.) and phosphorylated IP₃K-A-detected bands ($3.59 \pm 0.80\%$) suggesting that Ser-119-phosphorylated endogenous IP₃K-A does not bind to microtubules (Fig. 9D). Taken together, our results demonstrate that IP₃K-A is dissociated from microtubule by PKA-dependent Ser-119 phosphorylation (Fig. 9E).

DISCUSSION

IP₃K-A Is a Novel MAP Protein—In the present study, we identified tubulin as a novel binding protein of IP₃K-A through proteomic screening. Then, we confirmed its interaction by various *in vitro* and *in vivo* assays. Purified GST-IP₃K-A full-length protein was co-sedimented with purified microtubule *in*

IP₃K-A Binds Microtubule by PKA Phosphoregulation

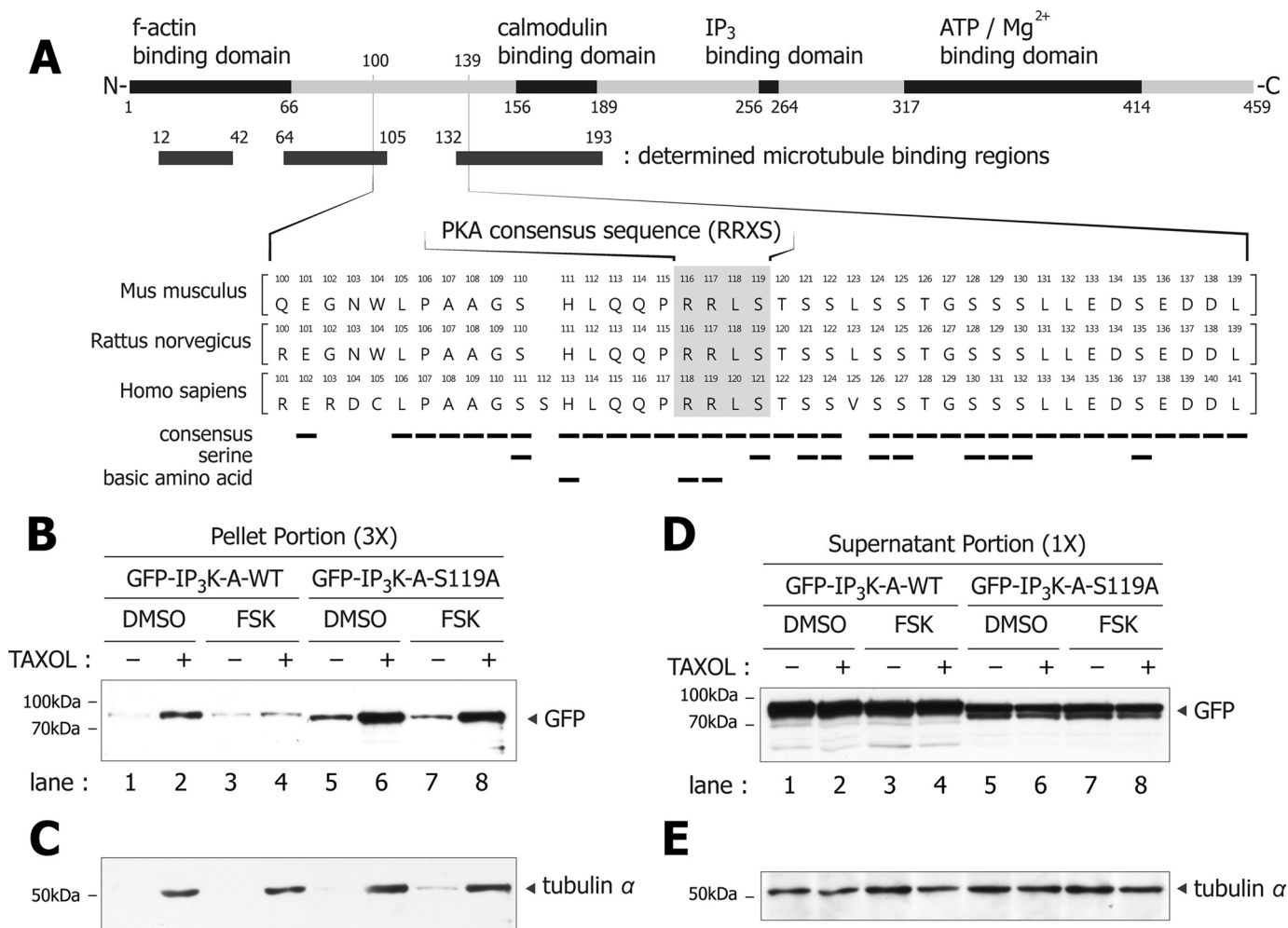


FIGURE 6. Interaction of microtubule with IP₃K-A is regulated by phosphorylation of IP₃K-A Ser119. *A*, amino acid sequence alignment of IP₃K-A from 100 to 139 including PKA consensus sequence. Note that amino acid sequences of human have two additional amino acids (Pro-89 and Ser-112), compared with rodent. All constructs in this study were originated from rat sequences. Consensus sequences, serine, and basic amino acids are denoted by *tiny solid bars*. *B*, immunoblotting analysis of tissue-based microtubule co-sedimentation assay of GFP-IP₃K-A-WT or S119A with microtubule. In pellet portions, GFP-IP₃K-A-WT (lanes 2 and 4) was less pelleted than GFP-IP₃K-A-S119A (lanes 6 and 8). Moreover, forskolin-treated GFP-IP₃K-A-WT (lane 4) was less pelleted than DMSO-treated GFP-IP₃K-A-WT (lane 2). *C*, pelleted tubulin levels were constant in the samples of GFP-IP₃K-A-WT and S119A. *D*, immunoblots of the supernatant portion in *in vivo* microtubule co-sedimentation. The pellet portion sample was three times more concentrated than the supernatant portion. *E*, supernatant portions of tubulin levels were nearly constant between GFP-IP₃K-A-WT and S119A.

in vitro microtubule co-sedimentation assay (Fig. 2*B*), indicating that it directly bound to the microtubule without the need for other proteins. Interestingly, GST-IP₃K-A increased the level of co-sedimented tubulin compared with GST control (Fig. 2*B*, lanes 6 and 12), suggesting that IP₃K-A may enhance microtubule polymerization or bundling. Although additional experiments are required, this finding raised the possibility that IP₃K-A could have the ability of microtubule bundling as well as F-actin bundling. Even though the dissociation constant of 3.99 μM (Fig. 2*D*) obtained from the binding curve between microtubule and IP₃K-A, this value was slightly higher than other MAPs, (tau: 0.15–0.57 μM (34), MAP2: 1–3 μM (35), doublecortin: ~ 2 μM (36)). However, this value is reasonable, considering the limitation of *in vitro* binding assay and the discrepancy of the experimental conditions.

Many MAPs bind to the acidic tail of α -tubulin through their basic amino acid residues such as lysine, histidine, and arginine (29). Indeed, IP₃K-A has many basic amino acid residues within its microtubule binding regions. This basic property of micro-

tubule binding region of IP₃K-A is clearly indicated by calculated isoelectric points (IP₃K-A N terminus aa 1–190, pI 10.125; IP₃K-A full-length, pI 7.584; tubulin α , pI 4.796; on-line site for calculation of isoelectric point), suggesting that electrostatic interactions are very important for their binding. Then the question arises how does Ser-119 phosphorylation interfere with the interaction of IP₃K-A with microtubule? One possible mechanism could be phosphorylation-induced conformational change, which masks microtubule binding regions. Inconsistent with this possibility, the IP₃K-A 106–131 deletion mutant, lacking Ser-119, still binds to microtubule (Fig. 5*C*), suggesting that this region does not directly contribute to the binding of microtubule or actually modulate conformational change. In addition, the microtubule binding region of IP₃K-A is relatively broad, therefore; it would be difficult to modify protein-protein interactions by a change in a single electrostatic interaction. To reveal the detailed mechanism, the full-length molecular structure of IP₃K-A, including its flexible N terminus, has to be resolved.

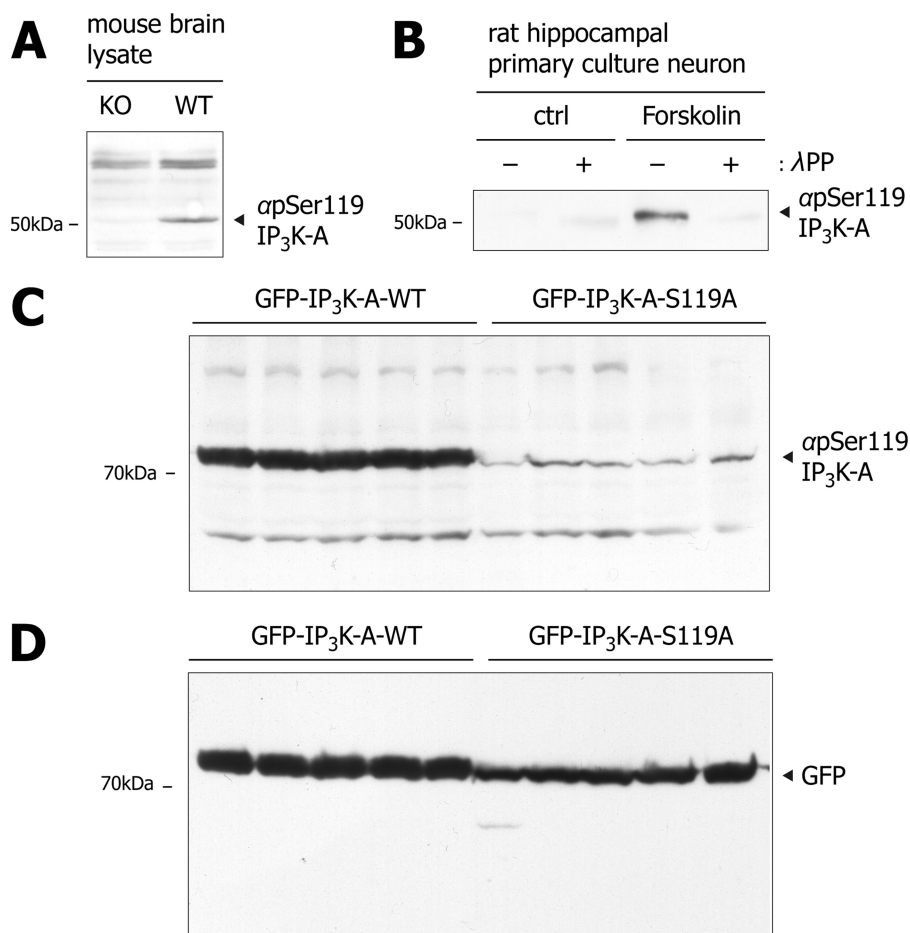


FIGURE 7. The generation and specificity of IP₃K-A pSer119 specific polyclonal antibody. *A*, immunoblots of rat brain lysates with IP₃K-A phosphoantibody (α pSer119 IP₃K-A). The polyclonal antibody was generated against phosphopeptide including pSer119. The specificity of α pSer119 IP₃K-A was confirmed using IP₃K-A knock and wild type mouse brain lysate. *B*, immunoblots of rat hippocampal culture lysates with α pSer119 IP₃K-A. α pSer119 IP₃K-A detected bands in forskolin-treated samples. α pSer119 IP₃K-A no longer detected compulsory dephosphorylated samples by lambda protein phosphatase (LPP). *C*, immunoblotting analysis of HEK293 cell lysates transfected either with GFP-IP₃K-A-WT or S119A, α pSer119 IP₃K-A specific blots were detected only in GFP-IP₃K-A-WT samples, indicating that our phosphoantibody detects the serine 119 phosphorylation specifically. *D*, immunoblotting with α GFP was used as a loading control.

PKA-dependent Phosphorylation of IP₃K-A and Interactions between IP₃K-A and Microtubules—*In vitro* kinase assay of IP₃K-A suggested that Ser-119 is phosphorylated by PKA, enhancing its enzyme activity (9, 11). However, there has been no direct evidence to indicate that this phosphorylation really occurs in the neuron. In this study, we demonstrated for the first time *in vivo* phosphorylation of Ser-119 using newly generated phosphoantibody (Fig. 8B). Considering the fact that PKA is involved in various forms of synaptic plasticity (37), PKA-dependent phosphorylation of IP₃K-A may play an important role in Ca²⁺-mediated signal transduction in synaptic plasticity by converting IP₃ to IP₄. IP₃ is known as an important second messenger that mediates Ca²⁺ release from the ER to the cytosol (38), while IP₄ is another messenger responsible for Ca²⁺ entry through the voltage-gated calcium channel (4, 39, 40). Previous electrophysiological studies showed that IP₃- and IP₄-mediated Ca²⁺ signaling is responsible for long-term synaptic plasticity. 2-APB (2-aminoethyl diphenyl borate), IP₃ receptor blocker, showed no LTP (41) and ω -conotoxin, N-type voltage-gated Ca²⁺ channel blocker, reduced LTP (42) in hippocampal slices, suggesting that local high concentrations of Ca²⁺ are important for LTP expression and that IP₃- and IP₄-

mediated signaling is necessary. Besides, changes in Ca²⁺ concentration could regulate microtubule polymerization rates (43, 44). Microtubules polymerize at low concentrations of Ca²⁺ whereas microtubules depolymerize at high concentrations of Ca²⁺. Therefore, PKA-dependent Ser-119 phosphorylation of IP₃K-A may mediate transient local calcium regulations for temporal regulation of synaptic plasticity and microtubule dynamics.

In addition, we found that PKA-dependent phosphorylation reduces the microtubule binding affinity of IP₃K-A (Figs. 8 and 9). So far, known functions in phosphorylation of IP₃K-A are limited to the regulation for its enzyme activity. The present study extends our knowledge and interests by revealing another role of IP₃K-A phosphorylation. This type of phosphoregulation is very similar to other MAPs; for example, tau, MAP2, and doublecortin (28–31). It is well known that dysregulation of MAP phosphorylation leads to diverse spectra of pathological effects, the most famous example being the hyperphosphorylation of tau induces the formation of neurofibrillary tangles in Alzheimer disease (28, 45). Many kinases are known to be involved in the phosphorylation of MAPs; for example, glycogen-synthase kinase 3 (GSK3), cyclin-dependent kinases

IP₃K-A Binds Microtubule by PKA Phosphoregulation

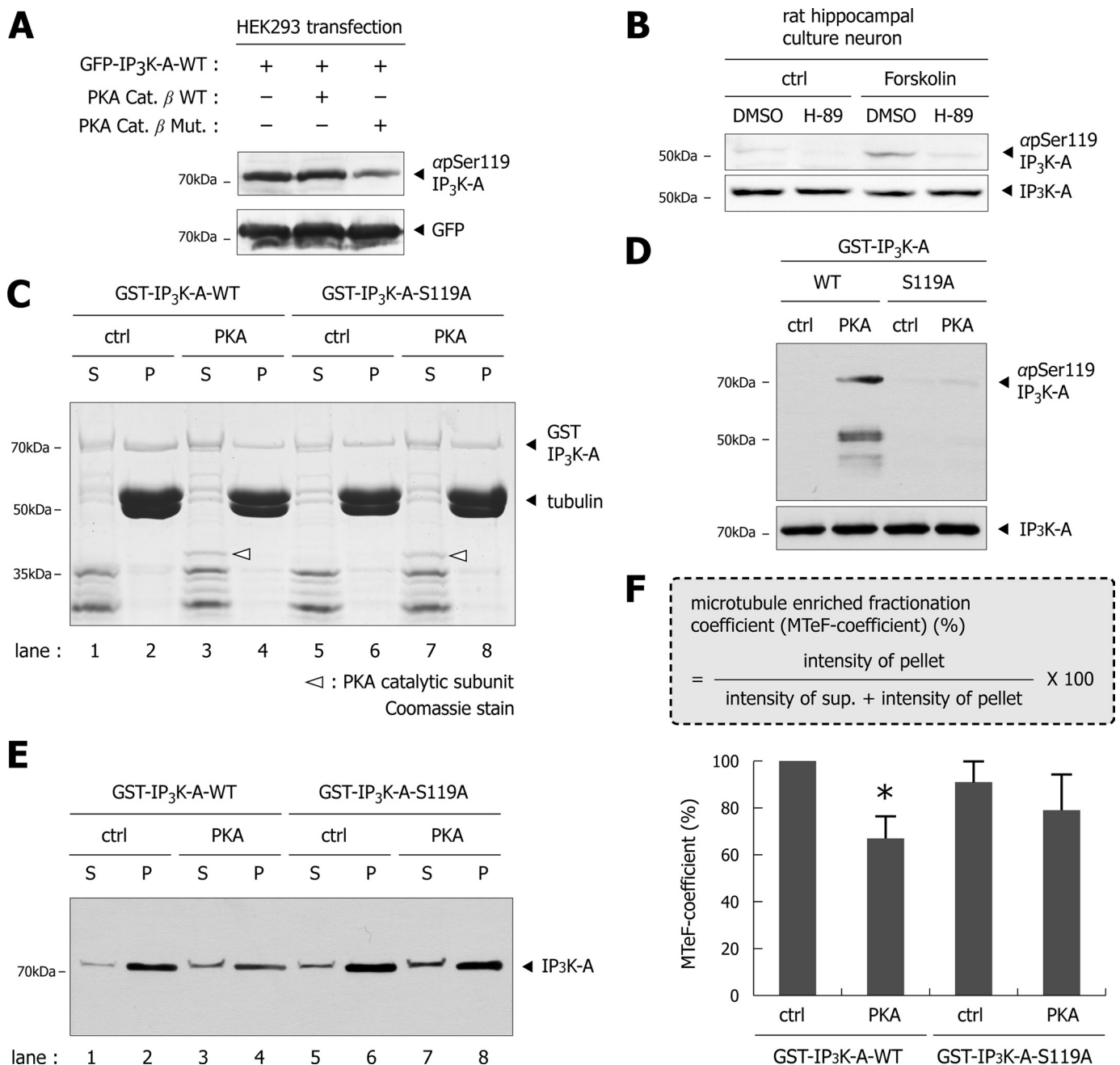


FIGURE 8. Catalytic subunit of PKA reduces microtubule binding affinity of IP₃K-A *in vitro*. *A*, immunoblotting analysis of HEK293 cell lysates. GFP-IP₃K-A was co-transfected with PKA catalytic subunit constructs (WT or kinase activity dead mutant). Immunoblotting with α GFP was used as a loading control. *B*, immunoblotting image of rat hippocampal culture lysates in the presence of 10 μ M H-89, a potent PKA inhibitor. Pretreatment of H-89 blocked Ser-119 phosphorylation despite forskolin (FSK; 50 μ M). Immunoblotting with total α IP₃K-A was used as a loading control. *C*, Coomassie-stained gel image of *in vitro* microtubule co-sedimentation assay in the treatment of PKA catalytic subunit. PKA catalytic subunit reduced microtubule binding affinity of GST-IP₃K-A-WT (lane 4), compared with control group (lane 2). GST-IP₃K-A-S119A was evenly pelleted (lanes 6 and 8), regardless of PKA catalytic subunit. Treated PKA catalytic subunit is denoted by a white arrowhead. *D*, effects of PKA catalytic subunits on IP₃K-A Ser-119 phosphorylation. Immunoblotting with total α IP₃K-A was used as a loading control. *E*, immunoblotting of *in vitro* microtubule co-sedimentation assay, show that band patterns are similar to the above Coomassie-stained gel image. *F*, microtubule-enriched fractionation coefficient (MTeF-coefficient) (%) = intensity of pellet portion / (intensity of supernatant portion + intensity of pellet portion) \times 100. Higher MTeF-coefficient means stronger microtubule binding affinity. The histogram shows statistically significant reductions of GST-IP₃K-A pelleting by the treatment of PKA catalytic subunits ($n = 3$, *, $p < 0.05$, one way ANOVA followed by Dunnett's test). Data are presented as mean \pm S.E.

(CDKs), microtubule-affinity-regulating kinases (MARKs), extracellular signal-regulated kinases (ERKs), CAMKII, PKC, and PKA (28–30). Particularly, PKA is involved in the phosphorylation of various MAPs, including tau, MAP2, and doublecortin (28–30). Interestingly, neuronal type II PKA binds indirectly to microtubule by MAP2-mediated interaction in the neuron (46), suggesting that

the microtubule may function as a kind of spatial compartment, mediating quick and efficient reactions of phosphorylation between PKA and its substrate, IP₃K-A.

Neuronal Function of PKA-dependent Phosphorylation of IP₃K-A and Interactions between IP₃K-A and Microtubules— How does PKA-dependent phosphorylation of IP₃K-A and

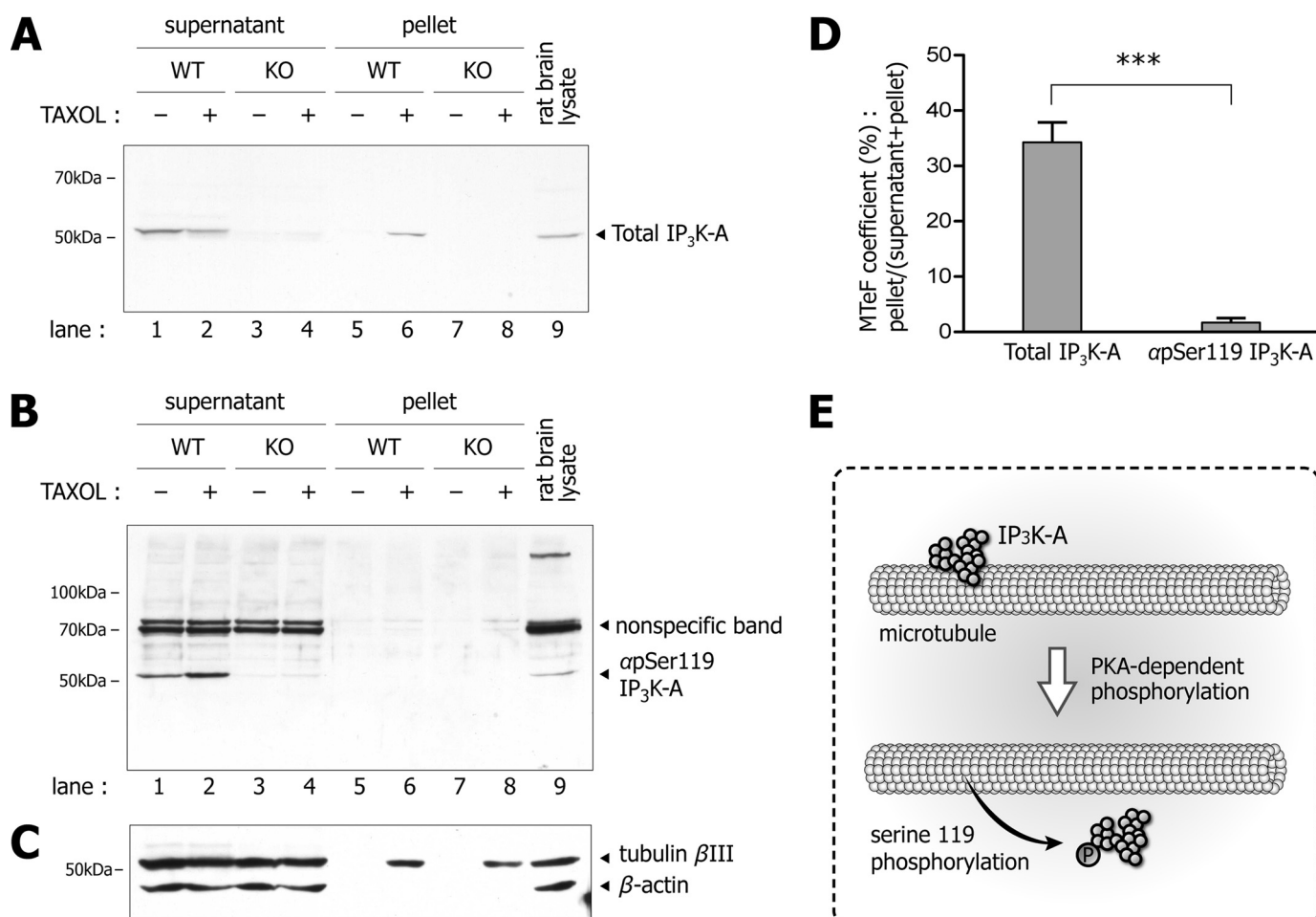


FIGURE 9. Phosphorylated endogenous IP₃K-A does not precipitate in tissue-based microtubule co-sedimentation assay. *A*, immunoblots of tissue-based microtubule co-sedimentation assay with IP₃K-A total antibody. Immunoblots of total IP₃K-A is detected in both supernatant (lane 2) and pellet (lane 6) fractions. We used both IP₃K-A-WT and KO mouse brain lysates to distinguish the real IP₃K-A band, because our pSer119 polyclonal antibody detected several nonspecific bands. *B*, immunoblots of pS119 IP₃K-A antibody were detected in the supernatant fraction (lane 2), not in the pellet fraction (lane 6). This discrepancy suggested that phosphorylated endogenous IP₃K-A does not bind to microtubule. *C*, blots with tubulin βIII and β-actin antibodies indicated that samples of microtubule-enriched fractionation were properly prepared. *D*, histogram of microtubule-enriched fractionation coefficient of IP₃K-A immunoblotting with total IP₃K-A and pS119 IP₃K-A antibodies. In these blots (independent experiments, $n = 3$), mean band intensity of total IP₃K-A was $34.25 \pm 4.08\%$ and that of pS119 IP₃K-A was $3.59 \pm 0.80\%$ MTeF-coefficient (Student's t test, $***, p < 0.001$). Data are presented as mean \pm S.E. *E*, schematic figure represents IP₃K-A dissociated from microtubule by PKA-dependent Ser-119 phosphorylation.

microtubule interactions contribute to neuronal functions? PKA plays critical roles in the integration and regulation of multiple synaptic events in long-term potentiation (LTP) (37, 47). We recently showed that IP₃K-A is accumulated in dendritic spines and reorganizes F-actin under chemical long-term potentiation (cLTP), thereby reorganizing F-actin and recruiting active Rac1 into dendritic spines (13). In the present study, we showed that PKA phosphorylated Ser-119 of IP₃K-A in the presence of forskolin (Fig. 8B). Considering that forskolin induces cLTP in hippocampus (48), Ser-119 phosphorylation and its microtubule dissociation may be involved in the spatial regulation of IP₃K-A. Similarly, Lfc, Rho-specific GEF (Guanine Nucleotide Exchange Factor), utilizes microtubules as its dendritic anchor for activity-dependent synaptic targeting (49). Additionally, PKA and EB3, microtubule plus end binding protein, also use microtubule as their dendritic anchors by MAP2-mediated binding (37, 50).

In conclusion, IP₃K-A is a novel MAP, and its microtubule binding affinity is negatively regulated by PKA-dependent

phosphorylation. Although physiological and cellular significances of microtubule binding of IP₃K-A and its phosphoregulation remain unclear, our findings may provide novel regulatory mechanisms for activity-dependent neuronal events such as synaptic targeting and local calcium signaling. Further study will focus on understanding the detailed molecular mechanisms responsible for IP₃K-A phosphorylation and its effect on synaptic plasticity.

Acknowledgment—We thank Dr. Woon Ki Paik (Temple University) for critical reading of this manuscript.

REFERENCES

- Lee, S. Y., Sim, S. S., Kim, J. W., Moon, K. H., Kim, J. H., and Rhee, S. G. (1990) Purification and properties of D-myo-inositol 1,4,5-trisphosphate 3-kinase from rat brain. Susceptibility to calpain. *J. Biol. Chem.* **265**, 9434–9440
- Choi, K. Y., Kim, H. K., Lee, S. Y., Moon, K. H., Sim, S. S., Kim, J. W., Chung, H. K., and Rhee, S. G. (1990) Molecular cloning and expression of

- a complementary DNA for inositol 1,4,5-trisphosphate 3-kinase. *Science* **248**, 64–66
3. Yamada, M., Kakita, A., Mizuguchi, M., Rhee, S. G., Kim, S. U., and Ikuta, F. (1993) Specific expression of inositol 1,4,5-trisphosphate 3-kinase in dendritic spines. *Brain Res.* **606**, 335–340
 4. Schell, M. J., Erneux, C., and Irvine, R. F. (2001) Inositol 1,4,5-trisphosphate 3-kinase A associates with F-actin and dendritic spines via its N terminus. *J. Biol. Chem.* **276**, 37537–37546
 5. Kim, I. H., Park, S. K., Sun, W., Kang, Y., Kim, H. T., and Kim, H. (2004) Spatial learning enhances the expression of inositol 1,4,5-trisphosphate 3-kinase A in the hippocampal formation of rat. *Brain Res. Mol. Brain Res.* **124**, 12–19
 6. Irvine, R. F., Letcher, A. J., Heslop, J. P., and Berridge, M. J. (1986) The inositol tris/tetrakisphosphate pathway—demonstration of Ins(1,4,5)P₃ 3-kinase activity in animal tissues. *Nature* **320**, 631–634
 7. Schell, M. J. (2010) Inositol trisphosphate 3-kinases: focus on immune and neuronal signaling. *Cell Mol. Life Sci.* **67**, 1755–1778
 8. Xia, H. J., and Yang, G. (2005) Inositol 1,4,5-trisphosphate 3-kinases: functions and regulations. *Cell Res.* **15**, 83–91
 9. Sim, S. S., Kim, J. W., and Rhee, S. G. (1990) Regulation of D-myo-inositol 1,4,5-trisphosphate 3-kinase by cAMP-dependent protein kinase and protein kinase C. *J. Biol. Chem.* **265**, 10367–10372
 10. Woodring, P. J., and Garrison, J. C. (1997) Expression, purification, and regulation of two isoforms of the inositol 1,4,5-trisphosphate 3-kinase. *J. Biol. Chem.* **272**, 30447–30454
 11. Communi, D., Vanweyenberg, V., and Erneux, C. (1997) D-myo-inositol 1,4,5-trisphosphate 3-kinase A is activated by receptor activation through a calcium/calmodulin-dependent protein kinase II phosphorylation mechanism. *EMBO J.* **16**, 1943–1952
 12. Windhorst, S., Blechner, C., Lin, H. Y., Elling, C., Nalaskowski, M., Kirchner, T., Guse, A. H., and Mayr, G. W. (2008) Ins(1,4,5)P₃ 3-kinase-A overexpression induces cytoskeletal reorganization via a kinase-independent mechanism. *Biochem. J.* **414**, 407–417
 13. Kim, I. H., Park, S. K., Hong, S. T., Jo, Y. S., Kim, E. J., Park, E. H., Han, S. B., Shin, H. S., Sun, W., Kim, H. T., Soderling, S. H., and Kim, H. (2009) Inositol 1,4,5-trisphosphate 3-kinase A functions as a scaffold for synaptic Rac signaling. *J. Neurosci.* **29**, 14039–14049
 14. Johnson, H. W., and Schell, M. J. (2009) Neuronal IP₃ 3-kinase is an F-actin-bundling protein: role in dendritic targeting and regulation of spine morphology. *Mol. Biol. Cell* **20**, 5166–5180
 15. Windhorst, S., Minge, D., Bähring, R., Huser, S., Schob, C., Blechner, C., Lin, H. Y., Mayr, G. W., and Kindler, S. (2011) *Cell Signal* **24**, 750–757
 16. Luo, L. (2000) Rho GTPases in neuronal morphogenesis. *Nat. Rev. Neurosci.* **1**, 173–180
 17. Hansson, M. D., Rzeznicka, K., Rosenbäck, M., Hansson, M., and Sirijovski, N. (2008) PCR-mediated deletion of plasmid DNA. *Anal. Biochem.* **375**, 373–375
 18. Hughes, J. R., Meireles, A. M., Fisher, K. H., Garcia, A., Antrobus, P. R., Wainman, A., Zitzmann, N., Deane, C., Ohkura, H., and Wakefield, J. G. (2008) A microtubule interactome: complexes with roles in cell cycle and mitosis. *PLoS Biol.* **6**, e98
 19. Paik, S. K., Bae, J. Y., Park, S. E., Moritani, M., Yoshida, A., Yeo, E. J., Choi, K. S., Ahn, D. K., Moon, C., Shigenaga, Y., and Bae, Y. C. (2007) Developmental changes in distribution of γ -aminobutyric acid- and glycine-immunoreactive boutons on rat trigeminal motoneurons. I. Jaw-closing motoneurons. *J. Comp. Neurol.* **503**, 779–789
 20. Bae, Y. C., Choi, B. J., Lee, M. G., Lee, H. J., Park, K. P., Zhang, L. F., Honma, S., Fukami, H., Yoshida, A., Ottersen, O. P., and Shigenaga, Y. (2002) Quantitative ultrastructural analysis of glycine- and γ -aminobutyric acid-immunoreactive terminals on trigeminal α - and γ -motoneuron somata in the rat. *J. Comp. Neurol.* **442**, 308–319
 21. Weber, K. L., Sokac, A. M., Berg, J. S., Cheney, R. E., and Bement, W. M. (2004) A microtubule-binding myosin required for nuclear anchoring and spindle assembly. *Nature* **431**, 325–329
 22. Tsukada, M., Prokscha, A., Ungewickell, E., and Eichele, G. (2005) Doublecortin association with actin filaments is regulated by neurabin II. *J. Biol. Chem.* **280**, 11361–11368
 23. Tsvetkov, A. S., Samsonov, A., Akhmanova, A., Galjart, N., and Popov, S. V. (2007) Microtubule-binding proteins CLASP1 and CLASP2 interact with actin filaments. *Cell Motil. Cytoskeleton* **64**, 519–530
 24. He, L., Zhang, Z., Yu, Y., Ahmed, S., Cheung, N. S., and Qi, R. Z. (2011) The neuronal p35 activator of Cdk5 is a novel F-actin binding and bundling protein. *Cell Mol. Life Sci.* **68**, 1633–1643
 25. Huang, S., Jin, L., Du, J., Li, H., Zhao, Q., Ou, G., Ao, G., and Yuan, M. (2007) SB401, a pollen-specific protein from *Solanum berthaultii*, binds to and bundles microtubules and F-actin. *Plant J.* **51**, 406–418
 26. Moseley, J. B., Bartolini, F., Okada, K., Wen, Y., Gundersen, G. G., and Goode, B. L. (2007) Regulated binding of adenomatous polyposis coli protein to actin. *J. Biol. Chem.* **282**, 12661–12668
 27. Roger, B., Al-Bassam, J., Dehmelt, L., Milligan, R. A., and Halpain, S. (2004) MAP2c, but not tau, binds and bundles F-actin via its microtubule binding domain. *Curr. Biol.* **14**, 363–371
 28. Johnson, G. V., and Stoothoff, W. H. (2004) Tau phosphorylation in neuronal cell function and dysfunction. *J. Cell Sci.* **117**, 5721–5729
 29. Sánchez, C., Díaz-Nido, J., and Avila, J. (2000) Phosphorylation of microtubule-associated protein 2 (MAP2) and its relevance for the regulation of the neuronal cytoskeleton function. *Prog. Neurobiol.* **61**, 133–168
 30. Schaar, B. T., Kinoshita, K., and McConnell, S. K. (2004) Doublecortin microtubule affinity is regulated by a balance of kinase and phosphatase activity at the leading edge of migrating neurons. *Neuron* **41**, 203–213
 31. Biernat, J., Gustke, N., Drewes, G., Mandelkow, E. M., and Mandelkow, E. (1993) Phosphorylation of Ser262 strongly reduces binding of tau to microtubules: distinction between PHF-like immunoreactivity and microtubule binding. *Neuron* **11**, 153–163
 32. Seamon, K. B., Padgett, W., and Daly, J. W. (1981) Forskolin: unique diterpene activator of adenylate cyclase in membranes and in intact cells. *Proc. Natl. Acad. Sci. U.S.A.* **78**, 3363–3367
 33. Maurer, R. A. (1989) Both isoforms of the cAMP-dependent protein kinase catalytic subunit can activate transcription of the prolactin gene. *J. Biol. Chem.* **264**, 6870–6873
 34. Goode, B. L., Chau, M., Denis, P. E., and Feinstein, S. C. (2000) Structural and functional differences between 3-repeat and 4-repeat tau isoforms. Implications for normal tau function and the onset of neurodegenerative disease. *J. Biol. Chem.* **275**, 38182–38189
 35. Coffey, R. L., and Purich, D. L. (1995) Non-cooperative binding of the MAP-2 microtubule-binding region to microtubules. *J. Biol. Chem.* **270**, 1035–1040
 36. Francis, F., Koulakoff, A., Boucher, D., Chafey, P., Schaar, B., Vinet, M. C., Friocourt, G., McDonnell, N., Reiner, O., Kahn, A., McConnell, S. K., Berwald-Netter, Y., Denoulet, P., and Chelly, J. (1999) Doublecortin is a developmentally regulated, microtubule-associated protein expressed in migrating and differentiating neurons. *Neuron* **23**, 247–256
 37. Zhong, H., Sia, G. M., Sato, T. R., Gray, N. W., Mao, T., Khuchua, Z., Haganir, R. L., and Svoboda, K. (2009) Subcellular dynamics of type II PKA in neurons. *Neuron* **62**, 363–374
 38. Berridge, M. J., Lipp, P., and Bootman, M. D. (2000) The versatility and universality of calcium signalling. *Nat. Rev. Mol. Cell Biol.* **1**, 11–21
 39. Fadool, D. A., and Ache, B. W. (1994) Inositol 1,3,4,5-tetrakisphosphate-gated channels interact with inositol 1,4,5-trisphosphate-gated channels in olfactory receptor neurons. *Proc. Natl. Acad. Sci. U.S.A.* **91**, 9471–9475
 40. Szinyei, C., Behnisch, T., Reiser, G., and Reymann, K. G. (1999) Inositol 1,3,4,5-tetrakisphosphate enhances long-term potentiation by regulating Ca²⁺ entry in rat hippocampus. *J. Physiol.* **516**, 855–868
 41. Gärtner, A., Polnau, D. G., Staiger, V., Sciarretta, C., Minichiello, L., Thoenen, H., Bonhoeffer, T., and Korte, M. (2006) Hippocampal long-term potentiation is supported by presynaptic and postsynaptic tyrosine receptor kinase B-mediated phospholipase C γ signaling. *J. Neurosci.* **26**, 3496–3504
 42. Baratta, M. V., Lamp, T., and Tallent, M. K. (2002) Somatostatin depresses long-term potentiation and Ca²⁺ signaling in mouse dentate gyrus. *J. Neurophysiol.* **88**, 3078–3086
 43. Fuller, G. M., and Brinkley, B. R. (1976) Structure and control of assembly of cytoplasmic microtubules in normal and transformed cells. *J. Supramol. Struct.* **5**, 497–514
 44. Schliwa, M. (1976) The role of divalent cations in the regulation of microtubule assembly. *In vivo* studies on microtubules of the heliozoan axopod

- dium using the ionophore A23187. *J. Cell Biol.* **70**, 527–540
45. Goedert, M. (2004) Tau protein and neurodegeneration. *Semin Cell Dev. Biol.* **15**, 45–49
46. Harada, A., Teng, J., Takei, Y., Oguchi, K., and Hirokawa, N. (2002) MAP2 is required for dendrite elongation, PKA anchoring in dendrites, and proper PKA signal transduction. *J. Cell Biol.* **158**, 541–549
47. Weisskopf, M. G., Castillo, P. E., Zalutsky, R. A., and Nicoll, R. A. (1994) Mediation of hippocampal mossy fiber long-term potentiation by cyclic AMP. *Science* **265**, 1878–1882
48. Otmakhov, N., Khibnik, L., Otmakhova, N., Carpenter, S., Riahi, S., Asrican, B., and Lisman, J. (2004) Forskolin-induced LTP in the CA1 hippocampal region is NMDA receptor dependent. *J. Neurophysiol.* **91**, 1955–1962
49. Ryan, X. P., Alldritt, J., Svenningsson, P., Allen, P. B., Wu, G. Y., Nairn, A. C., and Greengard, P. (2005) The Rho-specific GEF Lfc interacts with neurabin and spinophilin to regulate dendritic spine morphology. *Neuron* **47**, 85–100
50. Kapitein, L. C., Yau, K. W., Gouveia, S. M., van der Zwan, W. A., Wulf, P. S., Keijzer, N., Demmers, J., Jaworski, J., Akhmanova, A., and Hoogenraad, C. C. (2011) NMDA receptor activation suppresses microtubule growth and spine entry. *J. Neurosci.* **31**, 8194–8209